

THE EFFECT OF GLOBAL WARMING ON DYNAMICS, MICROPHYSICS AND ELECTRIFICATION OF CONVECTIVE CLOUD – NUMERICAL SIMULATIONS

BORYANA TSENOVA¹, RUMJANA MITZEVA², HRISTO IVANOV^{2,3}

¹ *National Institute of Meteorology and Hydrology, BAS*

² *Faculty of Physics*

³ *Chemical, Biological, Radiological and Nuclear Defense and Ecology, Musachevo, Bulgaria*

Боряна Ценова, Румяна Мицева, Христо Иванов. ВЛИЯНИЕ НА ГЛОБАЛНОТО ЗАТОПЛЯНЕ ВЪРХУ ДИНАМИКАТА, МИКРОФИЗИКАТА И НАЕЛЕКТРИЗИРАНЕТО НА КОНВЕКТИВЕН ОБЛАК – ЧИСЛЕНИ СИМУЛАЦИИ

Изследвано е влиянието на глобалното затопляне върху динамиката, микрофизиката и наелектризирането на мощен летен купесто-дъждовен облак с помощта на мезомасщабния модел MesoNH. Симулиран е случай на облак при използване на реален профил на температурата в околната среда и повишена температура с 3 и 5 градуса. Резултатите показват, че затоплянето не оказва съществено влияние върху динамиката на симулираните облаци. Повишаването на температурата води до увеличаване на масата на хидрометеорите в течна фаза и повишаване на акумулирания течен валеж, както и до съществена разлика в знака и разпределението на заряда, носен от различните хидрометеори.

Boryana Tsenova, Rumjana Mitzeva, Christo Ivanov. THE EFFECT OF GLOBAL WARMING ON DYNAMICS, MICROPHYSICS AND ELECTRIFICATION OF CONVECTIVE CLOUDS – NUMERICAL SIMULATIONS

The effect of global warming on summer convective cloud dynamics, microphysics and electrification is studied using MesoNH model. A cloud case is simulated using: a real temperature profile and warmer respectively with 3 and 5 degrees. Results show that warming does not affect significantly

For contact: Boryana Tsenova, NIMH, 66 Tsarigradsko chausse Blvd, GSM: +359 886 687 485, E-mail: boryana.tsenova@meteo.bg

cloud dynamics. The increase in temperature leads to an increase of liquid hydrometeors mixing ratio and of accumulated liquid precipitation, as well to significant differences in charge sign carried by different hydrometeors.

Keywords: global warming, convective clouds, numerical simulation, dynamics, microphysics, electrification

PACS numbers: 92.60 Pw, 92.60 Qx, 92.60 Ry

1. INTRODUCTION

The mean global surface temperature increases since the end of the 19th century [1]. The temperature increase was considerable between 1900 and 1940, as after 1970 until our days. However, this increase is not the same over the entire planet and in some places it is significantly higher than the defined global mean values. It is expected that the increase in temperature will have a significant impact on the development of convective clouds, thunderstorms and precipitation. Based on several studies such as [2–4] and others, it was stated [1] that the projected global warming will lead to more frequent and more severe extreme precipitation events. Trenberth et al. [5] studied the impact of various thermodynamical factors on precipitation, and concluded that the increased moisture content as a result of climate warming would have a significant impact on precipitation amount and intensity. Mccaul et al. [6] examined the sensitivity of supercell storms to environmental temperature and found that the updraft velocity and precipitation efficiency are higher at a colder environment, while the peak precipitation rate in a warmer environment is comparable to that in colder environment. Numerical simulations of Takemi et al. [7] with WRF model reveal the high dependence of the precipitation intensity from mesoscale convective systems on the temperature lapse rate. In the frame of their model simulations they found that with the increase of the lapse rate the mean precipitation intensity increases while the maximum precipitation intensity decreases. The author stresses on the need for diagnosis of stability in climate simulations and the need of further investigations on the effects of cloud microphysics on precipitation. Brandiyska et al. [8] using RAMS studied the effect of the expected changes of tropospheric temperature profile on the dynamical and microphysical characteristics of individual summertime convective storms and on the processes of precipitation development in these storms. Their results showed that projected warming lead to a decrease of precipitation from moderate cloud cases, while it leads to an increase of severe cloud cases precipitation. The main reason for the opposite direction of the impact of the projected tropospheric changes on different clouds lies in the ice phase evolution. The aim of the present study is to test the impact of expected changes in tropospheric temperature on convective clouds electrification having in mind the relationships between cloud electric charge structure and thundercloud microphysics and dynamics. Numerical simulations are performed using MésoNH model.

2. MÉSONH MODEL

The MésoNH is a non-hydrostatic mesoscale model developed in Laboratoire d'Aérodynamique and Météo-France [9]. The model integrates a system of equations able to simulate ideal and real atmospheric flows ranging from large eddy turbulent motion to the synoptic scale. The mixed-phase microphysical scheme in MésoNH follows the approach of Lin et al. [10] that is a three-class ice parameterization coupled to a Kessler scheme [11] used for the warm processes. The scheme follows the evolution of the mixing ratios of six water species: rv (vapour), rc and rr (cloud and rain drops) and ri , rs and rg (pristine ice, snow and graupel). The concentration of the precipitating particles is parameterized according to Caniaux et al. [12]. The pristine ice category is initiated by two heterogeneous nucleation processes: formation of ice embryos in a supersaturated environment over ice (deposition) following Meyers et al. [13], and freezing of supercooled droplets. In the model, the secondary production of ice crystals or rime-splintering mechanism is following Hallett and Mossop [14]. The homogeneous nucleation of pristine ice starts at temperatures lower than -35 °C. Ice crystals grow by water vapour deposition. The snow phase is initiated by autoconversion of primary ice crystals and it grows by deposition of water vapour, by aggregation through small crystal collection and by the riming produced by impaction of cloud droplets and of raindrops. Graupel particles are produced by the heavy riming of snow or by rain freezing when supercooled raindrops come in contact with pristine ice crystals. According to the heat balance equation and the efficiency of their collecting capacity, graupel particles can grow in dry and in wet mode (when riming is very intense and the excess of non-freezable liquid water at the surface of the graupel is shed and forms raindrops). At temperatures above 0 °C, ice particles melt into cloud and rain drops. Cloud droplet autoconversion, accretion and rain evaporation follow the Kessler scheme [11].

3. PARAMETERIZATION OF CHARGE SEPARATION IN THUNDERSTORM

The analytical expressions of the charging rates highly relies on the microphysical scheme:

$$\frac{dq_{xy}}{dt} = \int_0^{+\infty} \int_0^{+\infty} \left(\frac{\pi}{4} \delta q (1 - E_{xy}) (D_x - D_y)^2 (V_x - V_y) (n_x(D_x) n_y(D_y) dD_x dD_y) \right)$$

where D_x and D_y are the diameters for hydrometeors x and y , respectively. $|V_x - V_y|$ is the relative fall speed, n_x and n_y are the number concentrations of hydrometeors x and y , respectively, and E_{xy} is the collection efficiency. The collection efficiency depends on the temperature and follows Kajikawa and Heymsfield [15] for ice-snow and snow-graupel collisions and Mansell et al. [16] for ice-graupel collisions.

The expression of the charge exchanged is

$$\delta q = B d^a V^b \delta Q(RAR, T),$$

where B , a , and b are constants depending on the size of small ice particles, on the relative velocity V of the interacting ice particles, and on the sign of charge transfer and are tabulated in Saunders et al. [17]; δQ is the charge determined from the parameterization scheme for non-inductive charging proposed in Brooks et al [18] giving the relationships between the separated charge and cloud temperature T and rime accretion rate $RAR = EW \cdot V$, where EW is the effective water content.

$$\begin{aligned} \delta Q &= 6.74RAR - 1.36(-T) + 10.05 && \text{if } RAR > RAR_{cr}, \\ \delta Q &= 3.03 - 10.59RAR + 2.95RAR^2 && \text{if } 0 < RAR < RAR_{cr}, \end{aligned}$$

where $RAR_{cr} = -1.47 + 0.2(-T)$.

4. NUMERICAL SIMULATIONS AND RESULTS

For the aim of the study three cloud cases are simulated. For the case named as «original» or dT0 the sounding presented in Fig. 1a is used. The other two cloud cases are simulated using the modified according to Fig. 1b temperature profile. The modified soundings are named as dT3 and dT5 (the number 3 or 5 corresponding to an increase of surface temperature with 3 or 5 °C respectively). The sounding modification follows Santer et al. [19] findings that changes in temperature profile depend on latitude. According to Santer et al. [19] the increase in temperature is higher in upper troposphere. It is about 1.5 times higher than surface temperature increase and has a maximum at around 300 hPa. As there is not any consensus about changes in relative humidity profile [20], for our simulations it is assumed to be identical for cases dT3 and dT5 with dT0. By keeping relative humidity constant, it is clear that the specific humidity increases with the increase of temperature.

All simulations are performed over a domain of 25×20 km, 28 vertical levels, a horizontal step of 500 m with a perturbation of 1.5 °C and sizes of 10×10×2 km in the thermodynamic field. The simulations time is 40 min with a time step of 1s. For case dT0 the zero isotherm height is about 3.7 km, while for cases dT3 and dT5 about 4.0 and 4.5 km, respectively. The increase of the environmental temperature leads to an increase in altitude of the -40 °C isotherm, which means that the homogenous freezing of cloud water droplets is at higher altitude over the ground. For cloud case dT0 the height of -40 °C isotherm is at 9 km, while for dT3 — at 9.6 km, and for dT5 — at 10.5 km. Due to the presumption accepted here that relative humidity does not change with temperature changes, the lifted condensation level height is approximately the same for the three simulated clouds dT0, dT3 and dT5 (Table 1).

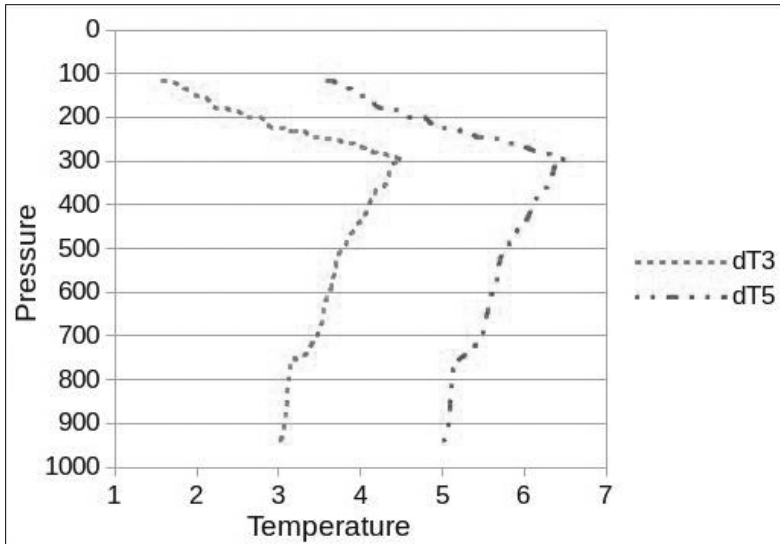
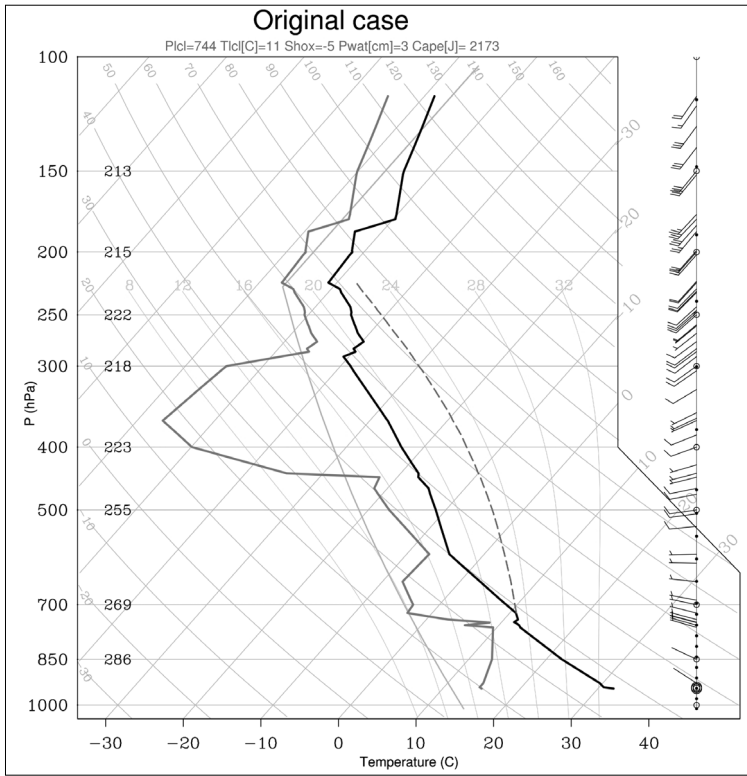


Fig. 1. a) Sounding used for case dT0 (original) simulation;
 b) temperature changes at different pressure height for cloud cases dT3 and dT5

Table 1. Height and temperature of lifted condensation level, CAPE and Lifted index for cloud cases dT0, dT3 and dT5

	dT0	dT3	dT5
Lifted condensation level height [m]	2717	2723	2727
Lifted condensation level temperature [°C]	11	14	16
CAPE [J/kg]	2173	2481	3162
Lifted index	-7	-7.4	-8.1

From Table 1 it is visible that cloud base for the three considered cases is at about 2.7 km. However the cloud base temperature for dT0 is 11 °C, while for dT3 and dT5 it is respectively with 3 and 5 °C warmer. The calculated CAPE and Lifted index based on soundings dT0, dT3 and dT5 show that for all considered cases the atmosphere is unstable and with temperature increase the instability increases significantly.

4.1. IMPACT OF TROPOSPHERE WARMING ON CONVECTIVE CLOUD DYNAMICS

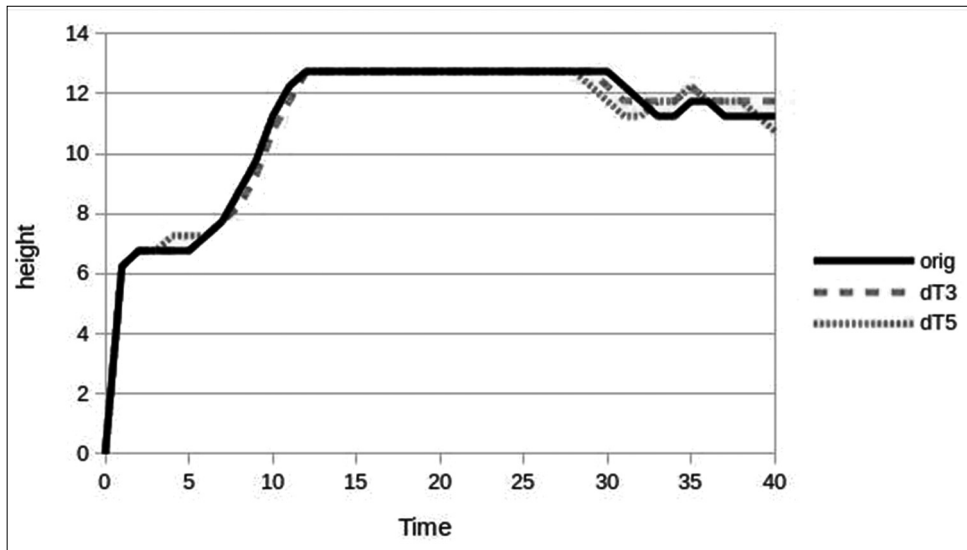


Fig. 2. Cloud cases dT0 (orig.), dT3 and dT5 top height AGL as a function of time after cloud case formation

Analysis shows that for the three considered cases condensation starts 5 min after the beginning of simulations. From Fig. 3 it is visible that the three simulated clouds tops increase during the following 13 min and until the 28 min, clouds tops are at the same height (about 12–13 km AGL). Despite the approximately same

altitudes of the simulated clouds tops, the lowest temperatures reached by the clouds are warmer with about 3 and 5 °C respectively for dT3 and dT5.

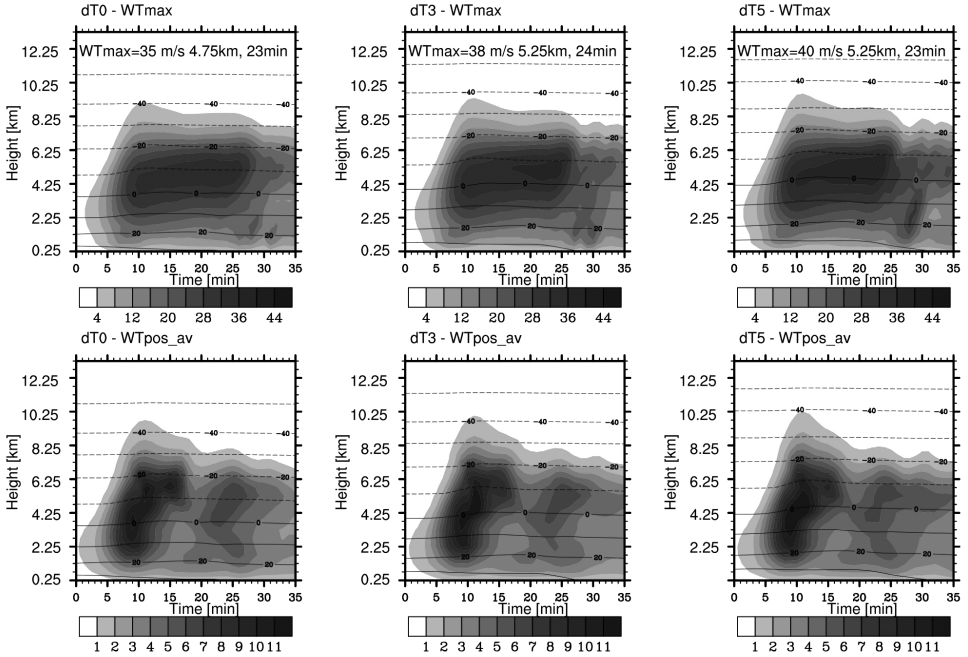


Fig. 3. Maximum updraft velocity, WTmax (top panel) and horizontally averaged updraft velocities, WTpos_av (bottom panel) as a function of time and height for the three cloud cases dT0, dT3 and dT5

During cloud development (Fig. 3, bottom panel) it is visible that for the three considered cloud cases the horizontally averaged updraft velocities WTpos_av are strong and between 23 and 28 min a second maximum is visible (at temperatures between +1 and -17 °C for dT0, between +2 and -12 °C for dT3, and for dT5 – between +5 and -10 °C). Results show that in warmer environments the maximum updraft velocity increases – it is 35 m/s for dT0, 38 m/s for dT3 and 40 m/s for dT5. These largest values of the maximum updraft velocity are reached between 23 and 24 min for the three considered clouds, at cloud temperature -7.5 °C for dT0, -7.4 °C for dT3 and -5.1 °C for dT5. Our results show that the increase in temperature profile has a weak effect on cloud dynamics leading to an increase of updraft velocity.

4.2. IMPACT OF TROPOSPHERE WARMING ON CONVECTIVE CLOUD MICROPHYSICS

Fig.4 shows the horizontally integrated mixing ratios in kg/kg of cloud and rain droplets as a function of time and height for the three simulated cloud cases dT0, dT3 and dT5. The horizontally integrated values of cloud water droplets in dT0 are lowest. The maximum mixing ratio $RC_{max} = 5.5$ g/kg is also the smallest in comparison with cases dT3 and dT5 (with RC_{max} respectively 7.1 and 7.9 g/kg) and it is reached at lowest altitude in the cloud (5.25 km) and latest (at 18 min after cloud formation). In dT3 and dT5 the maximum of RC is reached at higher altitudes (5.75 km and 6.25 km respectively). However, cloud temperatures are similar: -11 °C for dT0 and dT5 and -10 °C for dT3. In the three simulated cases there is cloud water until about -40 °C, which corresponds to an altitude of about 9 km for dT0, about 9.6 km for dT3 and about 10.2 km for dT5.

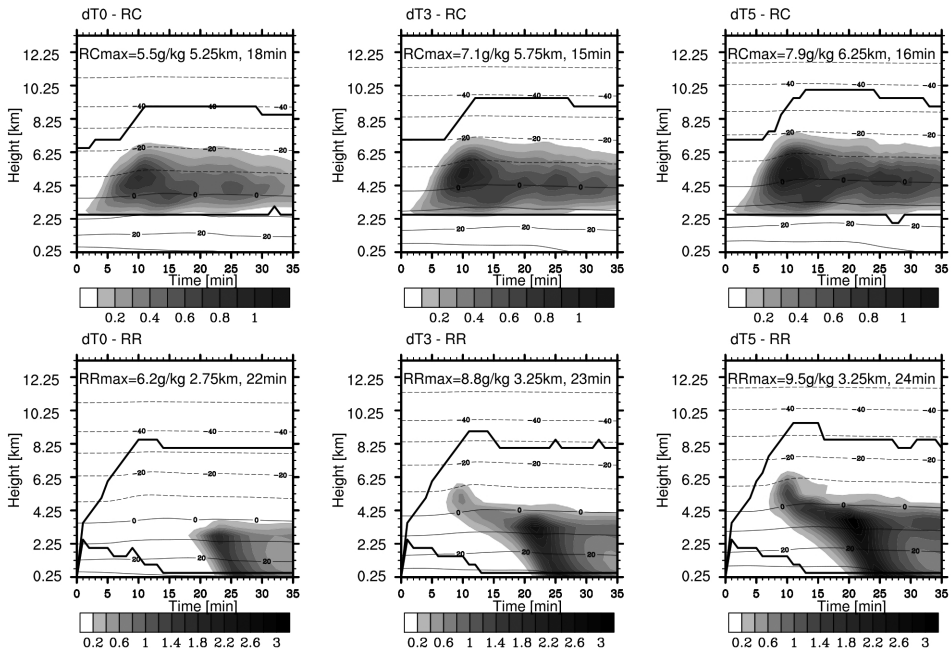


Fig.4. Horizontally integrated cloud, RC (top panel) and rain, RR (bottom panel) water droplets mixing ratios [kg/kg] as a function of time and height for the three considered cases dT0, dT3 and dT5 (the corresponding maximum values in g/kg are indicated above in each panel)

From Fig. 4 it is visible that the horizontally integrated rain water mixing ratio RR has high values at negative temperatures 10 min after cloud formation for cases dT3 and dT5, reaching 0.8 kg/kg and 1.2 kg/kg respectively, while for dT0 case it is below 0.2 kg/kg at negative cloud temperatures. For the three cases the maximum values of rain water mixing ratios are at positive cloud temperatures (at 6.5 °C, for dT0 and dT3 and at 9 °C for dT5). In case dT0 the value of maximum rain water mixing ratio is the lowest in comparison to dT3 and dT5 (respectively 6.2, 8.8 and 9.5 g/kg). Our results show that the increase of tropospheric temperature leads to an increase of liquid water (cloud and rain) mixing ratio in the simulated clouds. This result is not surprising, having in mind the higher cloud base temperature in clouds dT3 and dT5 in comparison to dT0 and the highest quantity of water vapour during clouds formation in warmer environment.

Fig. 5 shows the horizontally integrated mixing ratios in kg/kg of ice crystals, snow particles and graupel as a function of time and height for the three simulated cloud cases dT0, dT3 and dT5. It has to be stressed that at temperatures below -40 °C the mixing ratio of the horizontally integrated ice crystals is considerable in dT0, while at these cloud temperatures it is lower in dT3 and negligible in dT5. The maximum value of ice crystals mixing ratio in the three clouds is similar (about 1.7 g/kg). It is reached approximately at the same time (about 14 min after cloud formation) and at similar altitudes above ground level (about 8.5 km). However, the cloud temperature in the different clouds at the level of the maximum ice crystals mixing ratio achievement differs considerably. For dT0, R_{max} is reached at -33.6 °C; for dT3 — at -28.6 °C, and for dT5 — at -30 °C

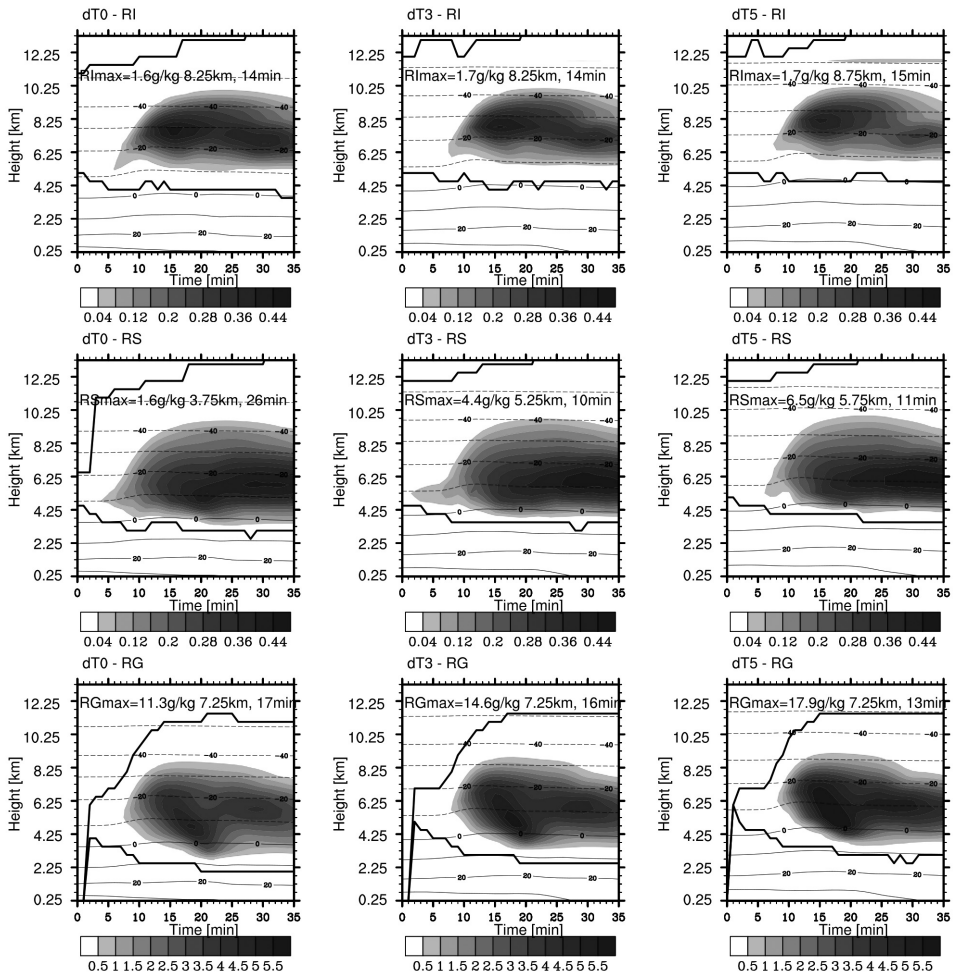


Fig. 5. Horizontally integrated ice crystals, *RI* (top panel), snow particles, *RS* (middle panel) and graupel, *RG* (bottom panel) mixing ratios [kg/kg] as a function of time and height for the three simulated cases dT0, dT3 and dT5 (the corresponding maximum values in g/kg are indicated above in each panel)

Similarly to ice crystals, horizontally integrated mixing ratios of snow particles are similar for the three cloud cases. However, in warmer environment the maximum of the horizontally integrated values of the mixing ratio are in a wider part of the cloud, for a longer time. The absolute maximum of snow particles mixing ratio *RS*_{max} differs considerably in the three clouds. In the coldest environment it has the lowest value, which is achieved latest and at lower altitudes. The maximum values of graupel mixing ratios (11.3 g/kg, 14.6 g/kg and 17.9 g/kg respectively for dT0, dT3 and dT5) are achieved at the same altitude (7.25 km), which corresponds

however to different cloud temperatures ($-26\text{ }^{\circ}\text{C}$, $-21\text{ }^{\circ}\text{C}$ and $-18\text{ }^{\circ}\text{C}$, respectively). Considering the horizontally integrated graupel mixing ratios for the three simulated clouds, one can see a second maximum, more pronounced for dT3 and dT5 cases, corresponding to the visible second maximum of horizontally averaged updraft velocities in Fig. 3 (bottom panel). Our results show that the increase in tropospheric temperature leads to an increase of snow and graupel mixing ratios.

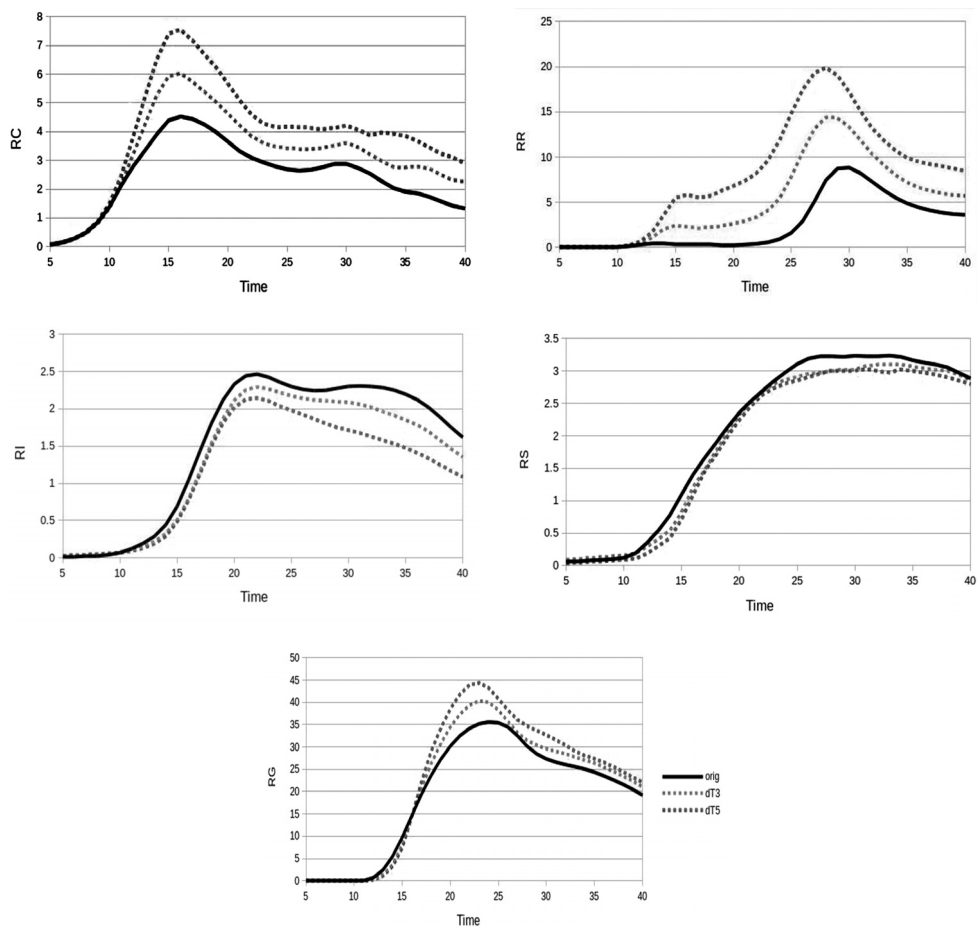


Fig. 6. Integrated cloud (RC) and rain (RR) water, ice crystals (RI), snow (RS) and graupel (RG) particles mixing ratios [kg/kg] as a function of time

The effect of tropospheric warming on integrated cloud water mixing ratio RC is well visible in Fig. 6. In the three simulated clouds, integrated cloud water is similar until the 12 min. Then, in warmer clouds dT3 and dT5 it increases considerably. Similar is the evolution of integrated rain water RR and graupel

RG mixing ratios that increase with temperature increase (Fig. 6). The effect of atmospheric warming on integrated ice crystals *RI* and snow *RS* mixing ratios is opposite, leading to their decrease. The increase of integrated rain water *RR* and graupel *RG* mixing ratios leads to higher values of liquid precipitation from dT3 and dT5 in comparison to dT0 (Table 2).

Table 2. Maximum accumulated liquid precipitation from the three simulated cloud cases dT0, dT3 and dT5

Simulated cloud cases	Maximum accumulated liquid precipitation [mm]
dT0	23.249
dT3	32.596
dT5	38.142

4.3. IMPACT OF TROPOSPHERE WARMING ON CONVECTIVE CLOUD ELECTRIFICATION

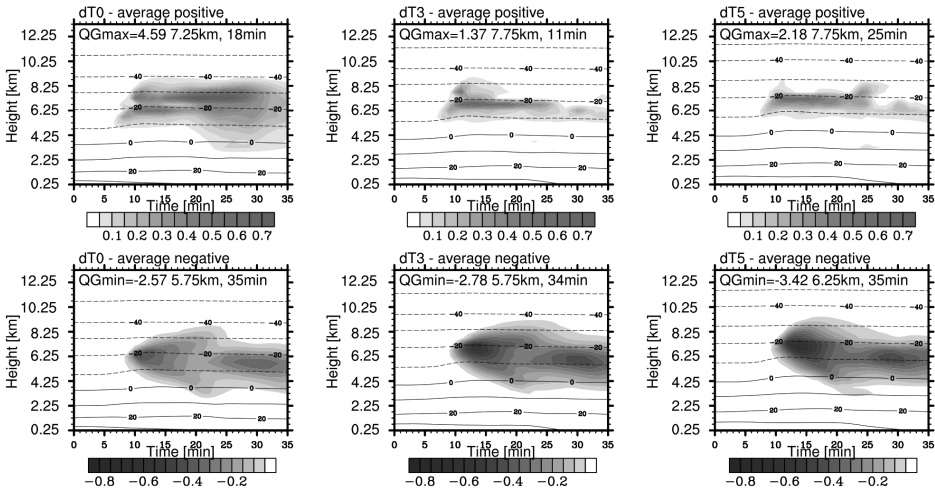


Fig. 7. Horizontally averaged positive (top panel) and negative (bottom panel) graupel charge density [nC/m^3] QG as a function of time and height for the three cloud cases dT0, dT3 and dT5 (the corresponding maxima as well time and height of their achievement are indicated above in each plot)

Fig. 7 shows the evolution of the horizontally averaged positive and negative graupel charge density for the three simulated cloud cases. It is visible that the average positive graupel charge density for dT0 case at temperatures below -20 °C after 15 min is larger than these in dT3 and dT5. Also Qgmax for this cloud case is considerably larger in comparison to the warmer clouds ($4.59 \text{ nC}/\text{m}^3$ for

dT0, while for dT3 and dT5 it is respectively 1.37 and 2.18 nC/m^3). The maxima positive graupel charge densities are achieved almost at the same height (about 7.5 km) in the three clouds, but the time of their achievements differs considerably (18 min, 11 min and 25 min respectively for dT0, dT3 and dT5). The tendency of the negative graupel charge density is opposite — there is a slight increase of maximum negative graupel charge density with the warming of the cloud. Our results show that the increase of tropospheric temperature leads to an increase of negative and to a decrease of the positive charge carried by graupel.

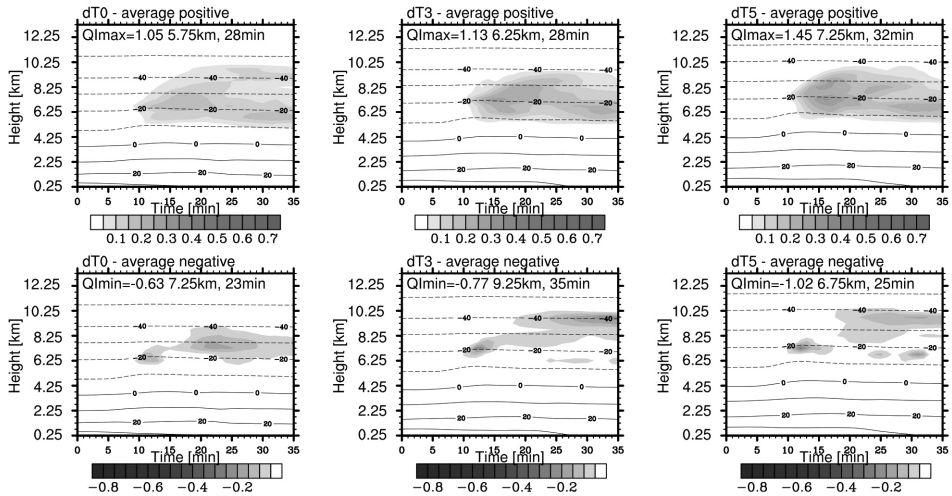


Fig. 8. Horizontally averaged positive (top panel) and negative (bottom panel) ice crystals charge density [nC/m^3] QI as a function of time and height for the three cloud cases dT0, dT3 and dT5 (the corresponding maxima as well time and height of their achievement are indicated above in each panel)

From Fig. 8. it is visible that the horizontally averaged positive ice crystals charge density in dT0 in the temperature interval $\langle -10, -40 \rangle$ °C is smaller than these in clouds developed in warmer environment. However, in this case the average positive ice crystals charge density at temperatures below -40 °C is bigger. There is a slight increase with the warming of the maximum positive (respectively 1.05 nC/m^3 , 1.13 nC/m^3 and 1.45 nC/m^3 for dT0, dT3 and dT5) as well of the maximum negative (-0.63 nC/m^3 , -0.77 nC/m^3 and -1.02 nC/m^3 for dT0, dT3 and dT5 respectively) ice crystals charge density.

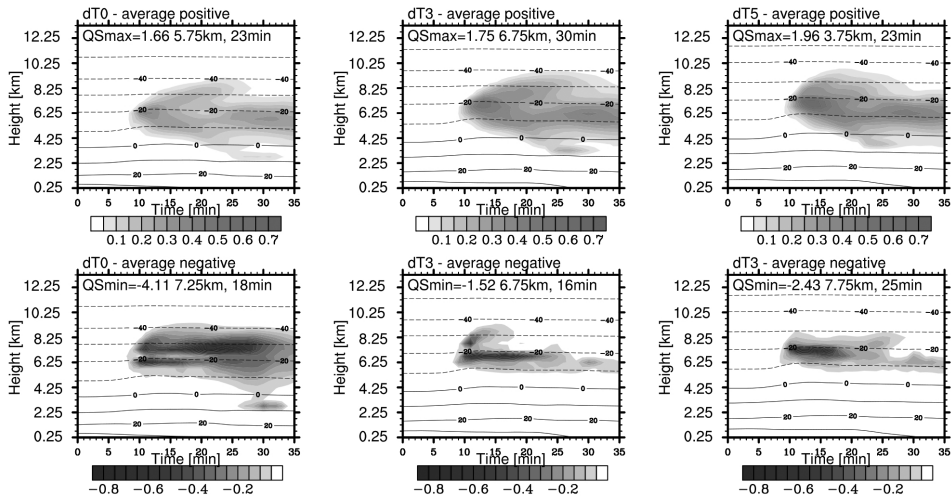


Fig. 9. Horizontally averaged positive (top panel) and negative (bottom panel) snow particles charge density [nC/m³] QS as a function of time and height for the three cloud cases dT0, dT3 and dT5 (the corresponding maxima as well time and height of their achievement are indicated above in each panel)

Fig. 9 shows the evolution of the horizontally averaged positive and negative snow particles charge density for the three simulated cloud cases. It is visible that at cloud temperatures above $-20\text{ }^{\circ}\text{C}$, the average positive snow charge density in dT0 is smaller in comparison to dT3 and dT5, while at temperature below $-20\text{ }^{\circ}\text{C}$, the average negative snow charge density is bigger in dT0. There is a slight increase of the maximum positive snow charge density with warming. The maximum negative snow charge density differs considerably in the three simulated cases: -4.11 nC/m^3 for dT0, -1.52 nC/m^3 for dT3 and -2.43 nC/m^3 for dT5. Our results show that the tropospheric warming leads to an increase of the positive and to a decrease of the negative charge density due to snow particles.

The analysis of cloud and rain water charge densities in the simulated cloud cases (not shown here) shows that the increase of tropospheric temperature leads to an increase of negative cloud water charge density and to a decrease of the positive rain water charge density.

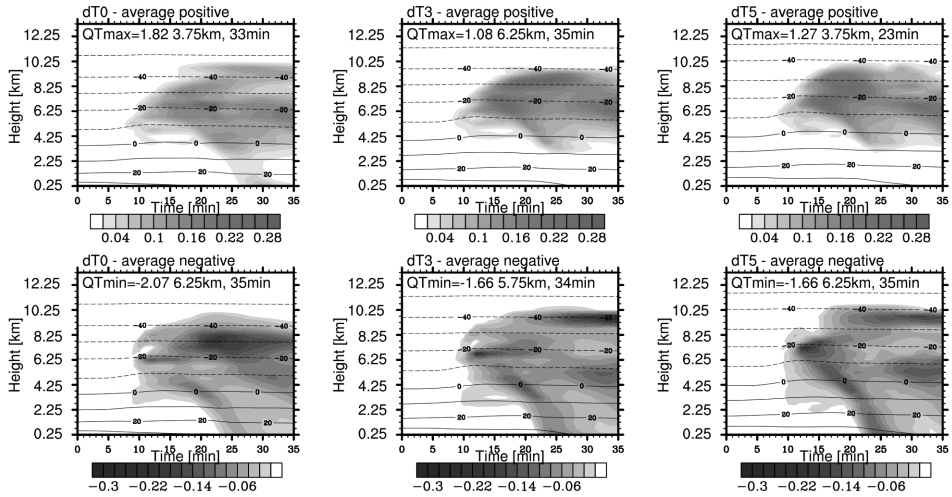


Fig. 10. Horizontally averaged positive (top panel) and negative (bottom panel) total charge density [nC/m^3] QT as a function of time and height for the three cloud cases dT0, dT3 and dT5 (the corresponding maxima as well time and height of their achievement are indicated above in each panel)

Fig. 10 shows the horizontally averaged positive and negative total charge density (which is the sum of the densities of the charges carried by all hydrometeors) as a function of time and height. From this figure one can see that warming leads to the increase of the average positive total charge densities, but to a decrease of its maximum values. The maximum and average negative total charge densities also decrease in clouds developed in warmer environment.

In Fig.11 the average total charge evolution for the three simulated cloud cases is presented. The main differences in cloud charge distribution between dT0 and the warmer dT3 and dT5 cloud cases are after 20 min. At temperatures between $-25\text{ }^\circ\text{C}$ and $-39\text{ }^\circ\text{C}$ the average total charge is negative in dT0, while in dT3 and dT5 it is positive.

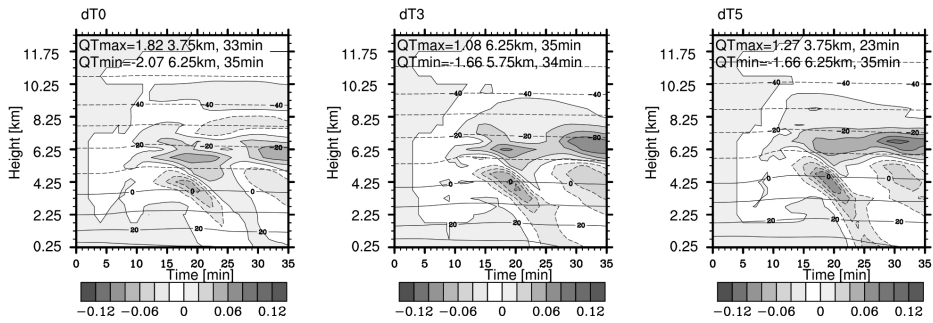


Fig. 11. Horizontally averaged total charge density [nC/m^3] QT as a function of time and height for the three cloud cases dT0, dT3 and dT5 (the corresponding maxima as well time and height of their achievement are indicated above in each panel)

This is a result of the higher negative charge density carried by snow particles in this cloud region in dT0 cloud in comparison to the warmer clouds. The average positive total charge density at positive temperatures in dT0 is due to the higher values of the positive rain water charge density in this cloud case. Our results show that tropospheric warming leads to an increase of the positive total charge density at negative cloud temperatures and to its decrease at positive cloud temperatures.

5. CONCLUSION

In the present study the impact of expected changes in temperature and humidity on thermodynamic and electrical characteristics of convective clouds is studied using the non-hydrostatic model MesoNH. Results show that the increase of temperature and specific humidity affects slightly the cloud dynamics in direction of updraft velocity increase. However, for the simulated cloud cases (the original one dT0, and the modified dT3 and dT5), there is no visible effect on their power, because their tops reach tropopause level and above the atmosphere is stable. Cloud development in warmer and more humid environment (dT3 and dT5) leads to an increase of liquid (cloud and rain) water and graupel mixing ratios. The increase of cloud and rain water mixing ratios can be explained by the higher water vapor mixing ratio in warmer cloud temperatures as are in dT3 and dT5 cloud cases. The higher concentration of cloud droplets in warmer clouds (dT3 and dT5) in comparison to the original (dT0) leads to an increase of graupel mixing ratio, as more cloud droplets freeze on riming graupel surface. The higher precipitating hydrometeors mixing ratios explain the visible increase of accumulated precipitation from the warmer clouds in comparison to the original. Our results are similar to those obtained in Brandiyska et al.[8].

Related to the impact of the warming on cloud electrification, our results show that it leads to:

- an increase of negative and a decrease of positive graupel charge density;
- an increase of maximum positive and negative charge carried by ice crystals;
- an increase of positive and a decrease of negative charge carried by snow particles;
- an increase of negative cloud droplets charge density and to a decrease of positive rain droplets charge density.

These results show that the warming of the troposphere affects in different directions the charging of the hydrometeors. As a result, the mean positive total charge density increases at negative temperatures and decreases at positive cloud temperatures. The warming leads to a decrease of maximum positive and negative total charge densities.

However, it has to be stressed that the results presented here are obtained for the simulated here cloud cases and following the presumption that the relative humidity will remain constant at global warming. However, if the humidity over continents does not increase enough to keep the relative humidity constant, the impact of such thermodynamical changes in the troposphere on convective clouds electrification will be less pronounced.

REFERENCES

- [1] IPCC, 2013: Climate Change: The Physical Science Basis. Contribution of Working Group I to the Fifth Assessment Report of the Intergovernmental Panel on Climate Change [Stocker, T.F., D. Qin, G.-K. Plattner, M. Tignor, S.K. Allen, J. Boschung, A. Nauels, Y. Xia, V. Bex and P.M. Midgley (eds.)]. Cambridge University Press, 2013, Cambridge.
- [2] Semenov, V. and L. Bengtsson. Report of the Intergovernmental Panel on Climate Change (IPCC), 2007.
- [3] Kharin, V. and F. Zwiers. Report of the Intergovernmental Panel on Climate Change (IPCC), 2007
- [4] Meehl, G. and others. Report of the Intergovernmental Panel on Climate Change (IPCC), 2007.
- [5] Trenberth, K, A. Dai, R. Rasmussen, and D. Parsons. *B.Am.Meteorol.Soc.*, 2003, **84**, 1205-1217.
- [6] McCaul, Jr., E.W., C. Cohen, C. Kirkpatrick. *Mon. Weather Re.*, 2005, **133**, 3015–3037.
- [7] Takemi, T. *Atmos. Res.*, 2010, **96**, 273-285.
- [8] Brandiyska, A., R. Mitzeva, B. Tsenova and J. Latham. *Idojaras*, 2012, **116**, 4, 253-280.
- [9] Meso-NH Scientific documentation version MASDEV4-10 (version August 20, 2014), <http://mesonh.aero.obs-mip.fr/mesonh52/BooksAndGuides>.
- [10] Lin, Y.-L., R. Farley, H. Orville. *J. Clim. Appl. Meteorol.*, 1983, **22**, 1065-1092.
- [11] Kessler, E. *Meteor. Monogr.*, 1969, Bolton, **10**, 32.
- [12] Caniaux, G., J.-L. Redelsperger, J.-P. Lafore. *J. Atmos. Sci.*, 1994, **51**, 046-2074.
- [13] Meyers, M.P., P. DeMott, W. Cotton. *J. Appl. Meteorol.*, 1992, **31**, 708-721.
- [14] Hallett, J., S. Mossop. *Nature*, 1974, 249, 26-28.
- [15] Kajikawa, M. and A. J. Heymsfield. *J. Atmos. Sci.*, 1989, **46** (20), 3108–3121.
- [16] Mansell, E. R., D. R. MacGorman, C. L. Ziegler, J. M. Straka. *J. Geophys. Res.*, 2005, **110**, D12101.
- [17] Saunders, C. P. R., W. D. Keith, R. P. Mitzeva. *J. Geophys. Res.*, 1991, **96**, 11007-11017.
- [18] Brooks, M., C. P. R. Saunders, R. P. Mitzeva, S. L. Peck. *J. Atmos. Res*, 1997, **43**, 277-295.
- [19] Santer, B.D, R. Sausen, T. Wigley, J. Boyle, A. Rao, K. Doutriaux, C. Hansen, J. Meehl, G. Roeckner, E. Ruedy, R. Schmidt and K. Taylor. *J.Geophys. Res.*, 2003, **108**, D1, 4001.
- [20] Elliot, W.P. and J. Angell. *Geophys. Res. Lett.*, 1997, **24**, 41-44